Journal of
MATERIALS RESEARCH

Article
DOI:10.1557/s43578-023-01198-0

Aluminum phosphate-based coatings: a novel approach to next generation of protective and thermal barrier coatings

F. S. Sayyedan[1,a)], **S. M. Nahvi**[1], **M. H. Enayati**[1]

[1] *Department of Materials Engineering, Isfahan University of Technology, 8415683111 Isfahan, Iran*
[a)] Address all correspondence to this author. e-mail: fs.sayyedan@alumni.iut.ac.ir

Received: 29 June 2023; accepted: 9 October 2023; published online: 25 October 2023

In the present study, a novel protective thermal barrier coating was developed. Amorphous aluminum phosphate powder was synthesized by sol–gel process and applied on Inconel 625 by air plasma spray (APS). Thermal conductivity of the compound was determined using laser flash analysis (LFA). The adhesion strength of the coating was evaluated by tensile test according to the ASTM-C633 standard. Hot corrosion behavior of the coatings was examined in Na_2SO_4–10 wt% NaCl molten salt at 1100 °C for 100 h. Thermal conductivity of the compound was obtained to be 1.1–2.2 W m^{-1} K^{-1} at 20–1000 °C which was considerably a low value compared to conventional TBC (8YSZ). The adhesion strength of the coating was obtained to be 40.8 ± 2 MPa which would be a significant value considering the applying method. The parabolic rate constant (K_p) for the coated sample was 23 times lower than that of the bare one after 100 h of exposure time.

Introduction

Thermal barrier coatings (TBCs) are classified as advanced materials commonly applied on metal surfaces used at high temperatures, such as turbine blades or aircraft engines to moderate significant temperature differences between the substrate and the coating. These coatings also increase the longevity of metal parts by mitigating corrosion and oxidation at high temperatures. The most famous of such a coating is Yttria-Stabilized Zirconia (YSZ) applied by thermal spraying on the substrate [1]. In general, many efforts are being employed to increase the efficiency and longevity of TBCs by improving the properties of known materials and achieving new materials.

For instance, the thermal conductivity of 7YSZ/$LaPO_4$ composite was evaluated for different amounts of monazite (0–17 wt%) and compared with the commercial 7YSZ powder. The value of thermal conductivity for 7YSZ at 1000 °C was 2.5 W/m K and reduced to 1.5 W/m K for 7YSZ/17$LaPO_4$ composite. However, the mechanical properties of the composite including hardness, elastic modulus, flexural strength, and fracture toughness decreased with addition of monazite particles to 7YSZ [2].

Fan et al. [3] designed the 7 mol% Sc_2O_3–0.5 mol% Y_2O_3–ZrO_2 (ScYSZ) composite to increase the thermal stability and decrease the thermal conductivity of 8YSZ. Although, the YSZ thermal conductivity reduced from 2.5 W/m K for 8YSZ to 1.9 W/m K for the ScYSZ composite, the elastic modulus and fracture toughness of the composite were accompanied with a slight drop.

Designing the YSZ/α-Al_2O_3 composite, Yang et al. [4] investigated the effect of addition of different amounts of alumina nanoparticles (20–80% vol%) on the thermal conductivity of 8YSZ at 50–900 °C. The thermal conductivity at 900 °C increased from 2.5 W/m K for 8YSZ to 7.5 W/m K for YSZ/α-Al_2O_3 composite with increasing the amount of alumina. Though alumina could improve the corrosion and oxidation resistance, increase the hardness and adhesion of the YSZ coating to the substrate with no obvious intervention in reducing fracture toughness and elastic modulus, YSZ/α-Al_2O_3 composite cannot be a suitable alternative to YSZ for thermal barrier applications. The coating hardness can even be improved by spraying an outer layer of aluminum oxide on the YSZ surface. However, the plasma-sprayed coating contains unstable phases of aluminum oxide including γ-Al_2O_3 and δ-Al_2O_3. The conversion of such phases to the α-Al_2O_3 stable phase during thermal cycles is accompanied with large volumetric changes (γ to α 15%) leading to the formation of cracks in the coating [5–7].

Although the most common TBC is YSZ, there are some other newest materials for high temperature applications. Mullite ($3Al_2O_3·2SiO_2$) owns superior oxidation resistance than YSZ. Due to the higher thermal conductivity of Mullite compared to YSZ, Mullite would be a suitable alternative to zirconia as a thermal insulation material in diesel engines with surface temperature lower than that of the gas turbines and wide temperature changes throughout the coating. The thermal instability of mullite and crystallization at temperatures below 1000 °C, followed by volume reduction, cracking in the coating, and separation from the substrate, are the main drawbacks in the use of Mullite-based coatings [8].

Cerium oxide has a higher thermal expansion coefficient and a lower thermal conductivity coefficient compared to YSZ and improves the thermal cycle life of YSZ coating due to limited tetragonal to monoclinic phase transformation, reduced stress in the bond coat oxidation by creating better thermal insulation, and a larger coefficient of thermal expansion in the $CeO_2 + YSZ$ coating. However, the YSZ/CeO_2 composite coating owns less hardness than the YSZ coating. Also, evaporation of CeO_2 at temperatures close to 1000 °C and conversion to Ce_2O_3, leads to a decrease in the protective effect of the coating followed by oxidation of the substrate [9, 10].

Among the broad group of silicates, the use of zircon ($ZrSiO_4$) as a thermal barrier coating has been reported. This material owns excellent corrosion and oxidation resistance. However, during the plasma spraying process, zircon decomposes into crystalline ZrO_2 and amorphous SiO_2. The thermal barrier properties are due to the zirconium oxide layer in the coating. However, if this material is used as a thermal barrier coating in diesel engines, the decomposed silica can cause issues in the coating due to the evaporation of SiO and $Si(OH)_2$ [11].

Rare earth oxides such as lanthanum oxide (La_2O_3), cerium oxide (CeO_2), dipraseodymium trioxide (Pr_2O_3), and niobium oxide (Nb_2O_5) are less expensive and readily available with lower thermal diffusivity and higher thermal expansion coefficient than ZrO_2 and good potential as a thermal barrier coating. However, most of these oxides undergo polymorphic transformation at high temperatures [12].

Roy et al. [13] deposited $AlPO_4$–C composite coating on the Ni-based supper alloy substrates by dip coating and spray coating techniques and evaluated cyclic oxidation resistance of the coatings in air at 800 °C and 1000 °C for 100 h of thermal exposure. The coatings with average thickness of 40 µm exhibited superior oxidation resistance compared to the bare substrates, so that the coated substrate showed slight weight change throughout the full oxidation cycle (100 h) indicating minimum oxidation of the coated substrate. In contrast, the bare substrate revealed substantial weight changes over the whole period of cyclic oxidation and underwent spallation multiple number of times. Although, the oxidation issue of the substrate can be resolved by employing dipped or sprayed coatings, it is clear that such a thin coating cannot meet the requirements as a thermal barrier coating.

Today, due to the increased demand of industries to increase the durability, performance, and efficiency of turbines, the need for progress in the production and upgrading of thermal barrier coatings is quite noticeable. Achieving advanced and modern thermal barrier coatings independent of the YSZ system with competitive and even superior properties and performance with lower cost, in terms of thermal insulation and protection against oxidation and corrosion at high temperatures, is the main goal and important consideration of the present research. Using less expensive and environmentally friendly raw materials with no heavy metals or environmental pollutants can meet well the needs of the industry. The new coating introduced in the present research is based on the combination of amorphous aluminum phosphate and can serve as a thermal barrier and protective coating on the surface of various substrates against oxidation and corrosion at high temperatures. Amorphous aluminum phosphate ($AlPO_4$) with low density (2.56 g/cm^3 for berlinite), high melting temperature (1800 °C), and high hardness (6.5 Mohs) can be considered as a promising anticorrosive coating material for a broad range of applications. Chemically inert nature and amorphous structure of $AlPO_4$ present excellent corrosion resistance due to the lack of crystalline defects such as grain boundaries [14]. Thus, in addition to enhancing the service life of the components, the efficiency of equipment operating at high temperatures improves with increasing temperature, leading to increased production per consumption of a certain amount of fuel with lower energy costs.

Results and discussion

SEM image of the synthesized aluminum phosphate powder along with the elemental analysis result of the powder after heat treatment at 500 °C for 30 min are presented in Fig. 1. Polygonal particles with faceted margins are immediately evident from SEM micrograph presented in Fig. 1. Image analysis using the ImageJ software revealed the powder particle size of 50–110 µm, the appropriate range for plasma spraying. EDS analysis of the synthesized powder after heat treatment at 500 °C for 30 min confirmed the presence of aluminum, oxygen, and phosphorus elements in the composition of the synthesized powder.

The X-ray diffraction patterns of the synthesized aluminum phosphate powder after heat treatment at 500 °C for 30 min (red pattern) and aluminum phosphate coating applied on Inconel 625 alloy (blue pattern) are shown in Fig. 2. One board hump is proud near 25° attributed to $AlPO_4$ phase. There is another hump around 70° attributed to α-Al_2O_3 phase raised from excess aluminum content in the precursor solution. Overall, the XRD pattern of the synthesized compound revealed that the sol–gel

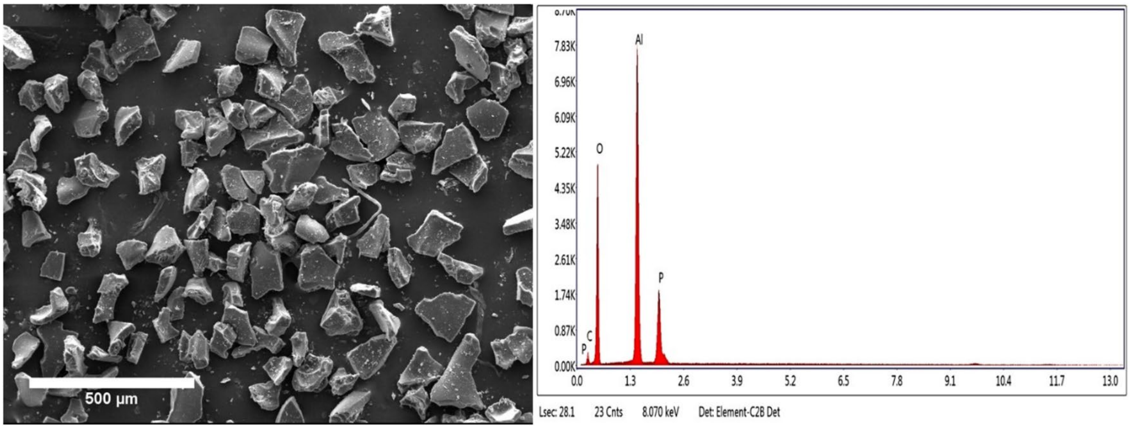

Figure 1: SEM image and EDS analysis of the synthesized aluminum phosphate powder after heat treatment at 500 °C for 30 min.

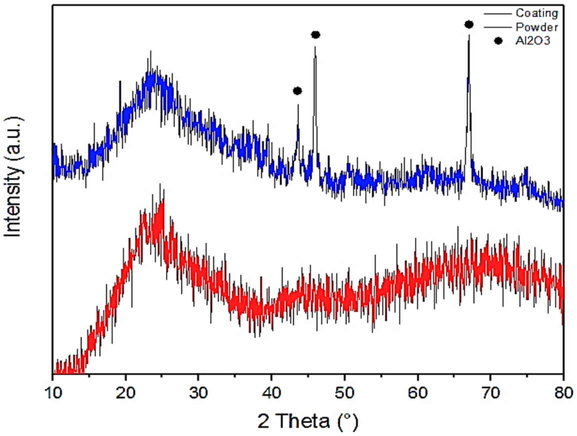

Figure 2: XRD patterns of aluminum phosphate coating applied on Inconel 625 alloy and synthesized aluminum phosphate powder after annealing at 500 °C for 30 min.

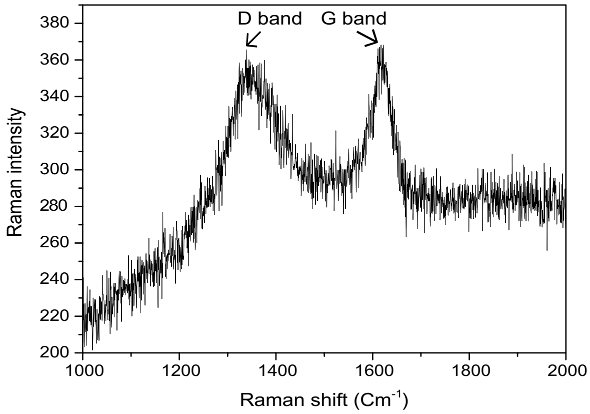

Figure 3: Raman spectrum of the synthesized aluminum phosphate powder after annealing at 500 °C for 30 min.

product did not have any crystalline characteristics, indicating the completely amorphous nature of the synthesized material. Moreover, the XRD pattern of the air plasma-sprayed coating does not show any symptoms of phase change or crystallization of the aluminum phosphate ($AlPO_4$) phase during spraying. By comparing the XRD patterns of the powder and the coating, the board hump in the range of 20°–30° is still visible in the diffraction pattern of the coating, which proves that the aluminum phosphate phase has retained its amorphous structure. The only difference in the diffraction pattern of the powder and the coating is the appearance of peaks related to corundum (α-Al_2O_3) in the diffraction pattern of the coating at angles of 43°, 46°, and 67° caused by the presence of excess aluminum content in the precursor solution compared to the stoichiometric composition and the high temperature (6000–15000 °C) during plasma spraying. Therefore, the coating contains an amorphous $AlPO_4$ matrix with α-Al_2O_3 crystalline particles. The presence of alumina in the composition of the coating not only improves the adhesion strength of the coating to the surface, but also provides good corrosion and oxidation resistance for the coating [15]. The effect of the presence of this phase in the coating composition will be discussed in the following sections.

The presence of carbonaceous phases in the sol–gel product was investigated by Raman spectroscopy. Figure 3 illustrates the Raman spectrum of the synthesized aluminum phosphate powder after annealing at 500 °C for 30 min. The peaks appeared at 1350 cm^{-1} and 1600 cm^{-1} are related to band D or irregularity in the graphite (amorphous carbon) and band G or the presence of graphite in the sample, respectively. The relative intensity of D band to G band is ID:IG = 0.97.

The presence of carbon in the aluminum matrix could be used as an index to confirm the following statements:

(1) The amorphous nature of this material: In other words, the carbon particles are completely encapsulated into the amorphous matrix. It is believed that the presence of carbon indicates the removal of oxygen from the C–O groups in ethanol by

aluminum and phosphorus atoms and the formation of $AlPO_4$ and Al_2O_3 crystallites.

(2) Low oxygen diffusivity in the substance: Because in the case of oxygen diffusion into the matrix, carbon should have left the inorganic matrix in the form of CO/CO_2.

The presence of carbon element in the coating material can bring high emissivity (thermal radiation) for the coating, which is very effective in thermal protection systems, such as aerospace. Thermal insulation coatings perform in the best way when the absorption-to-emission ratio is close to one, and in other words, the properties of the desired material are closer to the properties of the black body [16].

The values of specific heat capacity (C_p), thermal diffusivity (α), and thermal conductivity coefficient (K) of amorphous aluminum phosphate in the temperature range of 20–1000 °C are presented in Fig. 4. The temperature is increased continuously at a constant rate. According to Fig. 4(a), C_p increases with temperature. The ascending trend of the C_p–T curve could be an evidence of no phase changes for the substance during the temperature range of 25–1000 °C. As the substance heats up, the average kinetic energy of the molecules increments. The collisions confer enough energy to permit rotation to happen. Rotation at that point adds to the interior energy and raises the specific heat [17, 18].

As can be seen in Fig. 4(b), thermal diffusivity decreases with increasing temperature, which is due to the increase of phonon scattering. Crystal lattice oscillation (phonon) is the basis of heat transfer in ceramics. In other words, thermal conductivity in ceramics results from the interaction between phonons. According to the Debye formula (Eq. 1), thermal conductivity of solids (K) depends on specific heat capacity (C_p), speed of sound in solids (υ), and mean free path of phonons (the distance that phonons propagate without scattering) and electrons (L) [19].

$$K = 1/3L.C_p \cdot \upsilon. \tag{1}$$

The speed of phonons is largely independent of temperature, but the mean free path of phonons decreases with increasing temperature and reaches a minimum value depending on the distance between atoms. Therefore, increasing the phonon scattering and decreasing the mean free path with increasing temperature diminish the thermal diffusivity.

According to Fig. 4(c), the thermal conductivity coefficient of the synthesized aluminum phosphate from ambient temperature to 1000 °C is in the range of 1.1–2.2 W/m K, while this value has been reported to be 2.2–2.9 W/m K for the conventional thermal barrier coating (6–8 wt% yttria-stabilized zirconia) [20]. The low thermal conductivity value could be due to the amorphous nature of the material, followed by phonon conduction disturbance, and the presence of the carbon element in the composition of the material, which makes its properties close to those of the black body. Low thermal conductivity makes this material suitable as a durable thermal barrier coating for high temperature applications. According to Eq. (3), thermal conductivity is a function of thermal diffusivity and heat capacity of the material. The thermal diffusivity of amorphous aluminum phosphate according to the diagram presented in Fig. 4(b) is insignificant and decreases from 0.009 cm^2/s at ambient temperature to 0.006 cm^2/s at 1000 °C. Therefore, the dominant term in Eq. (3) for thermal conductivity is heat capacity, which increases with increasing temperature according to Fig. 5(a).

Figure 5(a) shows the SEM image of the plasma-sprayed amorphous aluminum phosphate coating on the Inconel 625. As can be seen, proper melting of particles, compact and

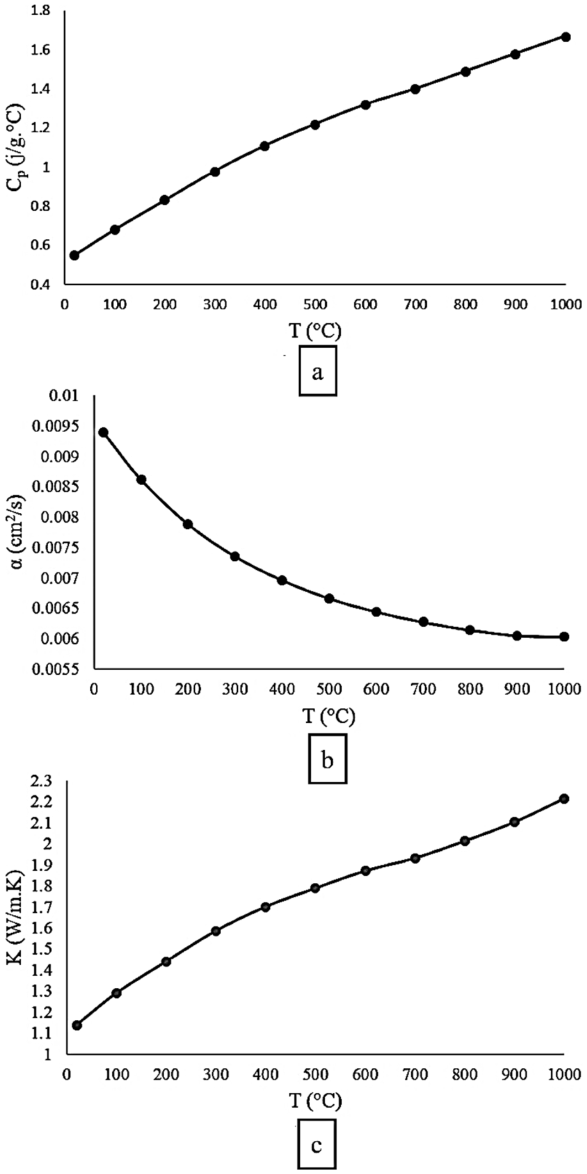

Figure 4: Values of (a) specific heat capacity (C_p), (b) thermal diffusivity (α), and (c) thermal conductivity coefficient (K) for amorphous aluminum phosphate at 20–1000 °C.

continuous coating with uniform thickness on the surface, and low porosity have been achieved by controlling the spraying parameters. Moreover, a good connection between the coating and the substrate followed by desired continuity between the coating layers (cohesion) are evident from Fig. 5(a). Image analysis by ImageJ software indicated that the average coating thickness was 150 ± 10 µm. Also, the percentage of the porosities of the coating was calculated to be ~ 1.5% with the average pore size of 5 µm [Fig. 5(b)]. The porosities are demonstrated by white arrows. This low porosity content (less than 2%) is usually attained by the High Velocity Oxygen Fuel (HVOF) spraying method. Porosity percentage values in the plasma spraying method have been generally reported to be in the range of 3–8% [21], although, more porosity values have also been obtained in some researches. For example, Aruna et al. [22] reported 11% porosity for 8 wt% yttria-stabilized zirconia coating applied by plasma spraying method on nickel-based super alloy. In another research, Sadeghi et al. [23] reported the porosity of 7 wt% yttria-stabilized zirconia coating to be 7% with an average pore size of 9 µm by optimizing the plasma spraying parameters.

The adhesion strength of the coating was investigated for two groups of coatings, namely without bond coat (group 1) and with bond coat (group 2). The force–displacement diagrams along with the adhesion strength values are presented in Fig. 6. Accordingly, the adhesion strength of the groups 1 and 2 were obtained to be 40.8 ± 2 MPa and 43.6 ± 2 MPa, respectively. Also, the graph presented in Fig. 6 revealed that the difference between the adhesion strength of coating with and without bond coat was negligible. In addition to the phosphatic nature of the coating and the presence of alumina particles in the coating structure, the favorable adhesion strength of the amorphous aluminum phosphate coating could be due to the presence of minimal porosity and un-melted particles in the coating structure [23]. Ghasemi et al. [24] studied the adhesion strength of 7 wt% yttria-stabilized zirconia coating on bond-coated low carbon Inconel 738 substrate. Their results showed that the adhesion strength values for conventional and nano-structured coatings were 25.35 MPa and 38.21 MPa, respectively. Other researchers reported an adhesive strength value of 30–40 MPa for the yttria-stabilized zirconia coating applied by plasma spraying [25, 26]. Adhesion strength values over 40 MPa could be achievable by HVOF method [27]. In general, the amount of adhesion strength depends on various factors including spraying parameters (spraying distance, gas flow rate, powder feeding rate, etc.), coating structure (percentage of porosities, oxides, un-melted particles, etc.), and coating thickness. The more value of adhesion would be achieved by reaching an optimal state of all conditions [28].

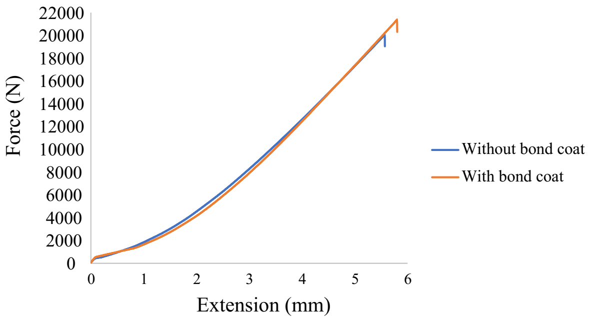

Figure 6: Force–displacement diagrams for amorphous aluminum phosphate coating on Inconel 625 alloy with and without bond coat.

The graphs of weight changes measured per unit area for uncoated Inconel 625 alloy and amorphous aluminum phosphate coating (with and without bond coat) versus time are presented in Fig. 7. It is noteworthy to mention that since the weight gain per unit area for the uncoated sample was 4.5 times greater

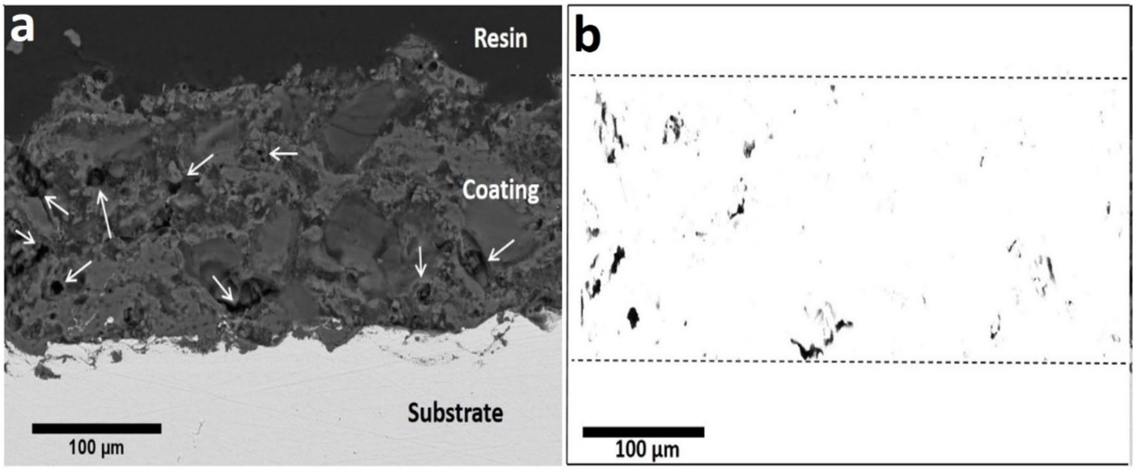

Figure 5: (a) Backscattered electron-SEM image of the cross section of the plasma-sprayed coating of amorphous aluminum phosphate powder on Inconel 625 and (b) porosity analysis using ImageJ software.

than that of the coated ones and they are presented in one diagram with the same vertical axis scale, graphs of weight change versus time for the coated samples were attached separately to Fig. 7 for clearer demonstration of the trend of weight change against time to detect the hot corrosion mechanism.

According to Wagner's theory, the corrosion/oxidation rate constant can be obtained by the slope of the graph of the weight change square per unit area versus time [29].

According to Fig. 7, the increase in the weight of the sample coated with amorphous aluminum phosphate (0.04 g/cm^2) and the sample coated with amorphous aluminum phosphate containing bond coat (0.1 g/cm^2) after 100 h of hot corrosion at 1100 °C are significantly less than that of the uncoated sample (0.45 g/cm^2) indicating the protective effect of the amorphous aluminum phosphate coating in the environment containing molten salt. It seems that the NiCoCrAlY bond coat has not played a significant role on the corrosion resistance of the substrate, and the surface protection against the molten salt environment was mainly due to the amorphous aluminum phosphate coating. This could be airside from the ability of the aluminum phosphate coating in the formation of thermally grown oxide (TGO) layer. As the XRD pattern of the coating (Fig. 2) shows, the peaks related to aluminum oxide corundum (α-Al_2O_3) appeared at angles of 43°, 46°, and 67° are related to the presence of excess aluminum content compared to the stoichiometry composition of $AlPO_4$ in the precursor solution. When the coating is exposed to the temperature of 1100 °C, the aluminum in the $AlPO_4$ composition turns into aluminum oxide (Al_2O_3) and creates a surface protective layer that protects the substrate from the aggressive corrosive environment. XRD patterns of the coating after the hot corrosion test (Fig. 8) also confirmed the presence of alumina phase on the surface of the coating. This phase content in aluminum phosphate coating is more significant in the absence of bond coat, while the dominant phases after the hot corrosion test in aluminum phosphate coating with bond coat are nickel–chromium spinel oxide ($NiCr_2O_4$) and $NiCrO_3$. It can also be seen that the intensity of the oxide peaks in the XRD pattern of Inconel 625 alloy is much higher than that of the coated samples and the dominant oxide is NiO.

According to Fig. 7, the graph of weight changes for both coated and uncoated samples follows a similar trend. Nevertheless, the kinetic effect of the coating on the corrosion behavior of Inconel 625 is quite obvious, as the weight gain of the uncoated substrate after 100 h of hot corrosion test (0.45 g/cm^2) is much higher than that for the coated sample (0.04–0.1g/cm^2) in the absence of bond coat and (0.1 g/cm^2) in its presence. By referring to the diagram presented in Fig. 7, it can be seen that the corrosion process of coated and uncoated Inconel 625 follows the parabolic velocity law according to Eq. (2) which indicates that the diffusion phenomenon across the thickness of the oxide layer controls the corrosion rate [29].

$$(\Delta W/A)^2 = a + k_p t, \tag{2}$$

where ΔW (g) is the weight change of the sample in each cycle, A (cm^2) is the surface area of the sample exposed to the corrosive environment, K_p (g^2 cm^{-4} h^{-1}) is the parabolic velocity constant, t (h) is the time, and a is a constant value.

By drawing weight change square per unit area graphs, two consecutive stages were observed for coated samples and one stage for uncoated sample, each of which followed the parabolic law (Fig. 7). In these graphs, the slope changes were observed

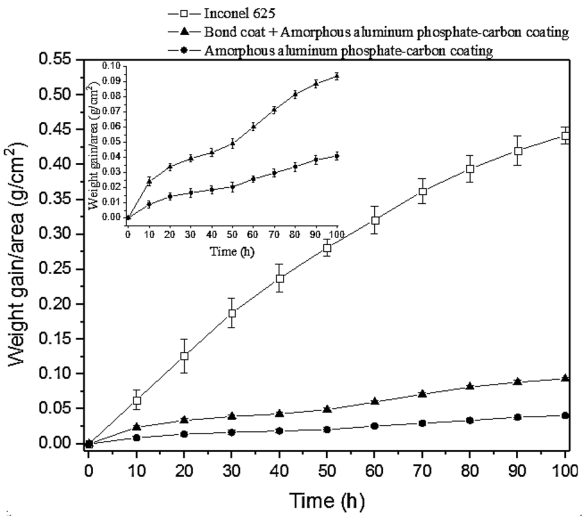

Figure 7: Graphs of weight change per unit area versus time for Inconel 625 substrate without coating and coated with amorphous aluminum phosphate with and without bond coat after 100 h of hot corrosion test at 1100°C (Appendix: Graphs of weight change versus time for amorphous aluminum phosphate coating with and without bond coat for clear demonstration).

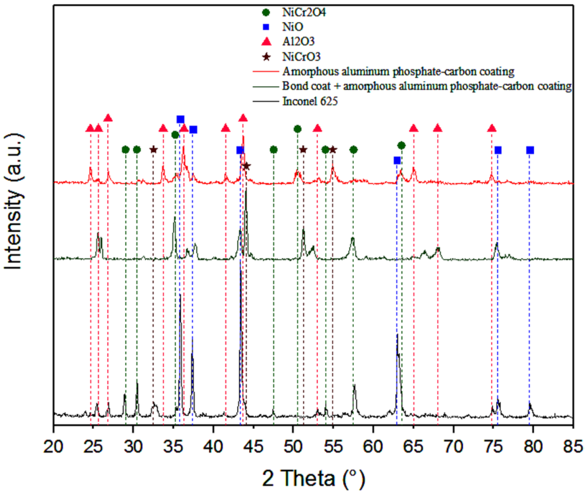

Figure 8: XRD patterns of Inconel 625 substrates without coating and coated with amorphous aluminum phosphate with and without bond coat after 100 h of hot corrosion test at 1100 °C.

after 50 h for coated samples. It can be seen that the weight gain of Inconel 625 was ~ 11 times greater than that of the amorphous aluminum phosphate coating without bond coat and ~ 5 times greater than that of the amorphous aluminum phosphate coating with bond coat.

While the K_p term for the bare Inconel 625 after 100 h of exposure time in the Na_2SO_4–10 wt% NaCl molten salt was measured to be 2×10^{-3} g^2 cm^{-4} h^{-1}, this value was obtained to be 2×10^{-4} g^2 cm^{-4} h^{-1} and 9×10^{-5} g^2 cm^{-4} h^{-1} for the amorphous aluminum phosphate coating with and without bond coat, respectively. Clearly, the K_p values for the coated substrate are significantly lower than that of the uncoated one, indicating the favorable corrosion resistance of the coating. It can also be seen that the K_p value for Inconel 625 is 22 times greater than that of amorphous aluminum phosphate coating without bond coat and 10 times greater than that of amorphous aluminum phosphate coating with bond coat. Superior corrosion resistance behavior of amorphous aluminum phosphate coating in the absence of bond coat will be better justified according to electron microscope observations and XRD pattern studies detailed in the next section.

SEM images and EDS analysis of the cross section of amorphous aluminum phosphate coating after hot corrosion test are shown in Fig. 9. Two red-marked areas in Fig. 10(a and c) are related to the EDS results presented in Fig. 10(b and d), respectively. The results represent a good agreement with the XRD patterns presented in Fig. 8. It should be mentioned that at the end of the 10th cycle of the hot corrosion test, the uncoated substrate was completely failed due to the formation and periodic peeling of the oxide layers and corrosion products, so that it was not possible to cross section the sample for SEM studies. The SEM cross-sectional image of the coating and EDS analysis (Fig. 9) shows that the metal surface area is mainly composed of aluminum oxide and some chromium oxide, while the amorphous aluminum phosphate coating with bond coat is mainly composed of chromium oxide at the end of the hot corrosion test [Fig. 10(c and d)]. By comparing images of Fig. 10(a and c), it could be seen that the amount of aluminum phosphate coating remaining at the distance of 200 μm from the surface was more significant for the sample without bond coat, while the coating containing NiCoCrAlY bond coat layer was subjected to more damage during the hot corrosion process. There are two origins for the formation of alumina layer on the surface of the coated substrate containing the bond coat layer, namely aluminum phosphate coating and bond coat. Therefore, the reason for the weaker corrosion resistance behavior of the coating containing the bond coat can be attributed to the greater thickness of the TGO layer

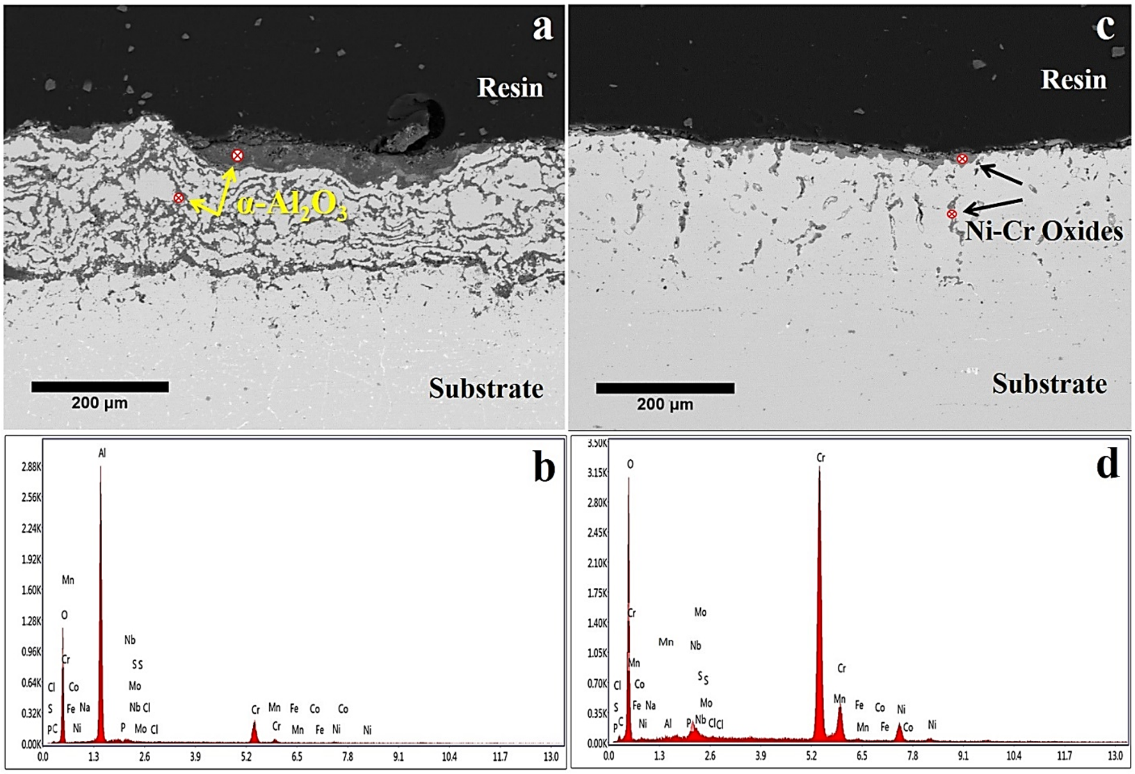

Figure 9: (a) SEM image of the cross section of the amorphous aluminum phosphate coating after 100 h of hot corrosion at 1100°C, (b) EDS analysis of the dark areas (marked points) in image a, (c) SEM image of the cross section of the amorphous aluminum phosphate coating with bond coat after 100 h of hot corrosion at 1100°C, (d) EDS analysis of the dark areas (marked points) in image c.

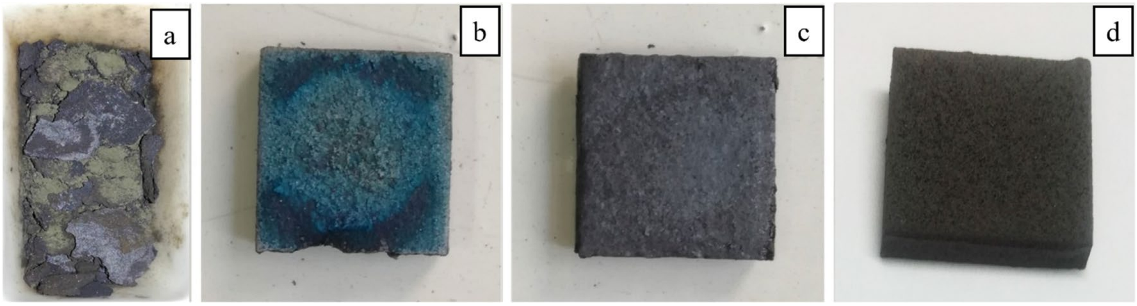

Figure 10: Surface images of uncoated Inconel 625 substrate (a) coated with amorphous aluminum phosphate and bond coat, (b) amorphous aluminum phosphate, (c) after 100 h of hot corrosion test at 1100°C, amorphous aluminum phosphate coating before hot corrosion test (d).

(α-Al_2O_3) followed by breaking and peeling from the surface of the substrate during the hot corrosion test which reduces the protective effect [14, 30, 31].

Figure 10 shows the images of the coated and uncoated Inconel 625 substrate after hot corrosion test. The outstanding difference in the appearance of the surface of the samples at the end of the 10th cycle indicates the significant difference in the corrosion resistance of the uncoated and coated substrates at high temperature. During different cycles of the hot corrosion test, the uncoated surface suffered from a large amount of weight gain, followed by significant cracking and peeling of the upper oxide layers and the formation of corrosion products. This phenomenon was observed with much lower intensity for coated substrates. On the other hand, the effects of scaling and formation of corrosion products on the coated surface with aluminum phosphate without bond coat were less evident compared to the sample containing NiCoCrAlY bon coat. As mentioned before, it was because of the greater thickness of the TGO layer in the sample containing bond coat followed by failure of this layer which reduces the protective effect.

In general, the results of adhesion and hot corrosion tests showed that the presence of NiCoCrAlY bond coat did not have a significant effect on improving the performance of the coating/substrate system in terms of adhesion and resistance to hot corrosion. Amorphous aluminum phosphate coating could provide desired properties including thermal insulation, adhesion, and hot corrosion resistance, simplifying the spraying process and reducing costs. This behavior was attributed to the phosphate nature of the amorphous aluminum phosphate coating and the presence of minimal porosity, defects, and unmelted particles in the structure of the coating and optimal adhesion on the surface, as well as the ability of the coating to form TGO (α-Al_2O_3) which provides good corrosion and oxidation resistance for the substrate. This new generation coating could be considered as a durable thermal barrier coating in a wide range of industries experiencing high temperatures over 1000 °C, such as aerospace, thermal power plants, oil, gas, and refining and petrochemical industries in order to protect the equipment, increasing the working temperature, or increasing the lifetime of metal parts.

Conclusions

In this research, amorphous aluminum phosphate powder was synthesized by sol–gel process and coated on Inconel 625 super alloy by APS method with a thickness of 150 µm. The main results were obtained as follows:

1. The adhesion strength of the coating without bond coat was obtained to be 40.8 MPa, which was remarkable considering the coating method (APS) and absence of bond coat.
2. The porosity of the coating was less than 2%, which was unique considering the coating method (APS).
3. The presence of carbonaceous species in the synthesized aluminum phosphate composition offered high emissivity (thermal radiation) for the coating followed by thermal insulation property.
4. The thermal conductivity of the coating material at 20–1000 °C was obtained to be 1.1–2.2 W/m K, which was well comparable to the thermal conductivity values reported for the most common thermal barrier coating, 8YSZ.
5. The coating in the absence of bond coat with K_p value of 3×10^{-5} g^2 cm^{-4} h^{-1} had a very good corrosion resistance in the molten salt Na_2SO_4–10 wt% NaCl at 1100 °C for 100 h, which was 23 times lower than that of the bare Inconel 625.
6. The amorphous aluminum phosphate coating was able to form a protective and adhesive TGO layer (α-Al_2O_3) at elevated temperature, providing hot corrosion resistance without the need of bond coat.

Materials and methods

In order to synthesize amorphous aluminum phosphate powder by sol–gel process, Aluminum nitrate nonahydrate ($Al(NO_3)_3{\cdot}9H_2O$, PENTA, 98.5%) and phosphorus pentoxide (P_2O_5, PENTA, 99.5%) were dissolved separately in ethanol

(C_2H_5OH, PENTA, 99.9%) with a molar ratio of Al/P:1.75/1. After complete dissolution, the two solutions were mixed and homogenized using a magnetic stirrer. In order to distribute the raw materials uniformly and accelerate the hydrolysis process, the above solution was mixed for one hour at ambient temperature and one hour at 50 °C by a magnetic stirrer. In order to complete the hydrolysis and polymerization processes of the precursors and sufficient opportunity for the ions to be evenly distributed in the structure, the aging operation was performed at room temperature for 24 h. The resulting gel was dried at 100 °C in an oven to reach a fluffy gel. The dried gel was heat-treated in a programmable electrical furnace (Nobertherm N7/H, Germany) at 500 °C for 30 min to reach amorphous aluminum phosphate powder.

The synthesized amorphous aluminum phosphate powder was milled in an alumina mortar and then separated by sieves with mesh number of 140 and 270 to make the particle size suitable for plasma spraying (53–106 μm). Inconel 625 sheet with a thickness of 3 mm was cut in to a size of 15 mm × 15 mm and then sand blasted with alumina particles with a mesh size of 24. Coatings were applied by plasma spraying gun (GTV Verschleiss-Schutz GmbH, Germany). The parameters used for spraying of amorphous aluminum phosphate powder and AMDRY 365–2 Sulzer Metco powder with the composition of Ni23Co17Cr13Al0.5Y (wt%) as bond coat are presented in Table 1. It should be noted that the coatings were classified in two groups, namely with and without bond coat.

X-ray diffraction (Philips X'Pert-MPD System) analysis was employed to identify the phase composition of the synthesized powder and the coatings using CuKα beam ($\lambda_{CuK\alpha} = 0.154$ nm, radiation at 40 kV and 40 mA) over the 2θ range of 20°–85°. X'Pert HighScor and OriginPro 2017 software (Version: 1.0d) were used for phase detection and qualitative analysis of diffraction patterns.

The morphology and elemental analysis of the synthesized powder and plasma-sprayed coatings were investigated by scanning electron microscope (Philips XL30, Netherlands) equipped with an X-ray energy-dispersive spectroscopy (EDS). The porosity of the coating was analyzed and calculated by ImageJ software version 1.47.

TABLE 1: Parameters used for plasma spraying process of amorphous aluminum phosphate powder and NiCoCrAlY powder as bond coat.

Powder	Current (A)	Voltage (v)	Hydrogen gas flow rate (L/min)	Argon gas flow rate (L/min)	Spraying distance (cm)
Amorphous aluminum phosphate	630	68	12	35	9
NiCoCrAlY	650	42	8	50	14

Raman spectroscopy (Horiba Jobin–Yvon LabRam HR-800) was used in the range of 2000–11000 cm^{-1} to investigate the carbonaceous phases in the synthesized aluminum phosphate composition. The laser excitation and laser power were adjusted at 514 nm and 0.1 mW, respectively.

The adhesion strength of the coating to the substrate was evaluated using the tensile test according to the ASTM-C633 standard test method. Accordingly, cylindrical samples with a diameter of 25 mm and a height of 40 mm were prepared. The surface of the cylinders was sand blasted and classified in two groups, namely with and without bond coat, and then subjected to plasma spraying. The coated cylinders were coaxially connected to another similar cylinder using high-strength epoxy resin adhesive with 75 MPa adhesion strength and cured at 150 °C for 180 min. The two connected pieces were subjected to axial loading by a tensile apparatus (Hounsfield, H25KS, England) and pulled off at a rate of 0.8 mm/min until failure. Adhesion strength was calculated from the ratio of the failure force to the failure cross-sectional area. Tensile test was repeated for three samples in each group and the average of the obtained values was reported as the adhesive strength.

Thermal conductivity of the synthesized amorphous aluminum phosphate was determined using laser flash analysis method (Netzsch LFA 457, Selb, Germany) according to the ASTM E1461-13 standard test method in the temperature range of 20–1000 °C in argon atmosphere. Amorphous aluminum phosphate powder was compacted in to disc-shaped samples with a diameter of 12.7 mm and a thickness of 2 mm using spark plasma sintering method. The porosity and relative density of the bodies were obtained to be 1.5% and 98.5%, respectively. One surface of the sample was exposed to laser radiation while temperature changes were recorded on the counterpart surface. Thermal conductivity (K, W/m K) was calculated using Eq. (3) at each temperature.

$$K = \alpha \cdot \rho \cdot C_p, \tag{3}$$

where α (m^2/s) is thermal diffusivity, ρ (kg/m^3) is density, and C_p (j/kg K) is specific heat capacity.

Hot corrosion behavior of the coatings in Na_2SO_4–10 wt% NaCl molten salt medium was examined in a programmable electrical furnace (Carbolite S30 2AU, England) at 1100 °C for 100 h in air. Five sides of the coupons were masked with a heat-resistant adhesive up to 1500 °C (Selsil ®, Turkey) to expose only the upper surface to the corrosive environment. The coupons were put in to an oven at 150 °C for a short period of time to cure the adhesive. The samples were placed in separate alumina crucibles and 5 mg/cm^2 of the fresh salt mixture was poured on the upper surface of the samples in each cycle. The set was heated up to 1100 °C and let cool in the furnace to reach the room temperature. The weight changes of the coated and uncoated substrates (three samples in each group) including corrosion products were measured after each ten-hour regular interval by an electrical balance with an accuracy of ± 0.1 mg. The weight change per unit area (ΔW/A) was calculated according to Eq. (4). It is notable that

$$\Delta W/A = (W_{\mathrm{i}} - W_0)/A, \tag{4}$$

where W_i is the weight of the sample after each cycle, W_0 is the initial weight of the sample, and A is the surface area of the sample exposed to the corrosive environment.

Acknowledgments

The authors greatly appreciate the support of Technology Innovation and Commercialization Center located at Isfahan University of Technology on this research.

Author contributions

FSS (Conception, Experimental design, Carrying out measurements, and Manuscript composition), SMN and MHE (Supervision and Manuscript review).

Funding

Not applicable.

Data availability

Data will be made available on request.

Declarations

Conflict of interest There are no conflicts of interest or competing interests.

References

1. J.G. Thakare, C. Pandey, M.M. Mahapatra, R.S. Mulik, Thermal barrier coatings—a state of the art review. Met. Mater. Int. **27**, 1947 (2021)
2. X. Ren, S. Guo, M. Zhao, W. Pan, Thermal conductivity and mechanical properties of YSZ/$LaPO_4$ composites. J. Mater. Sci. **49**(5), 2243 (2014)
3. W. Fan, Z.Z. Wang, Y. Bai, J.W. Che, R.J. Wang, F. Ma, W.Z. Tao, G.Y. Liang, Improved properties of scandia and yttria co-doped zirconia as a potential thermal barrier material for high temperature applications. J. Eur. Ceram. Soc. **38**(13), 4502 (2018)
4. F. Yang, X. Zhao, P. Xiao, Thermal conductivities of YSZ/Al_2O_3 composites. J. Eur. Ceram. Soc. **30**(15), 3111 (2010)
5. A.Z.A. Azhar, M.M. Ratnam, Z.A. Ahmad, Effect of Al_2O_3/YSZ microstructures on wear and mechanical properties of cutting inserts. J. Alloys Compd. **478**(1), 608 (2009)
6. X. Luo, Z. Ning, L. Zhang, R. Lin, H. He, J. Yang, Y. Yang, J. Liao, N. Liu, Influence of Al_2O_3 overlay on corrosion resistance of plasma sprayed yttria-stabilized zirconia coating in NaCl-KCl molten salt. Surf. Coat. Technol. **361**, 432 (2019)
7. J. Yao, Y. He, D. Wang, Influence of Al_2O_3/YSZ micro-laminated coatings on high temperature oxidation and spallation resistance of MCrAlY alloys. J. Phys. Conf. Ser. **419**(1), 012019 (2013)
8. P. Ramaswamy, S. Seetharamu, K.J. Rao, K.B.R. Varma, Thermal shock characteristics of plasma sprayed mullite coatings. J. Therm. Spray Technol. **7**(4), 497 (1998)
9. A. Dragomirescu, N. Constantin, A. Ştefan, V. Manoliu, R. Truşcă, Advanced study of thermal behaviour of CSZ comparing with the classic YSZ coating. IOP Conf. Ser.: Mater. Sci. Eng. **163**(1), 012040 (2017)
10. W. Xiao, Q. Guo, E.G. Wang, Transformation of CeO_2(111) to Ce_2O_3(0001) films. Chem. Phys. Lett. **368**(5), 527 (2003)
11. R.S. Pavlik Jr., H.J. Holland, E.A. Payzant, Thermal decomposition of zircon refractories. J. Am. Ceram. Soc. **84**, 2930 (2001)
12. X. Cao, Application of rare earths in thermal barrier coating materials. J. Mater. Sci. Technol. **23**(01), 15 (2007)
13. S. Roy, S.R. Reddy, P. Sindhuja, D. Das, V.V. Bhauprasad, $AlPO_4$-C composite coating on Ni-based super alloy substrates for high emissivity applications : experimentation on dip coating and spray coating. Def. Sci. J. **66**(4), 425 (2016)
14. F.S. Sayyedan, M.H. Enayati, M. Hashempour, A. Vicenzo, M. Bestetti, Synthesis and characterization of sol-gel derived non-stoichiometric aluminum phosphate coating. Surf. Coat. Technol. **351**, 128 (2018)
15. H. Xu, H. Guo, S. Gong, *Thermal Barrier Coatings, in Developments in High Temperature Corrosion and Protection of Materials* (Elsevier, Amsterdam, 2008), p.476
16. Z. Yao, X. Li, H. Wei, Q. Xia, Y. Wang, D. Li, Z. Jiang, Black ceramic coatings on Ti alloy with enhanced high absorptivity and high emissivity by plasma electrolytic oxidation. Int. J. Appl. Ceram. Technol. **16**, 994 (2019)
17. Y. He, Heat capacity, thermal conductivity, and thermal expansion of barium titanate-based ceramics. Thermochim. Acta **419**(1), 135 (2004)
18. H. Wen, J.-H. Lu, Y. Xiao, J. Deng, Temperature dependence of thermal conductivity, diffusion and specific heat capacity for coal and rocks from coalfield. Thermochim. Acta **619**, 41 (2015)
19. J. Chen, Y. Long, X. Xiong, P. Xiao, Microstructure and thermal conductivity of carbon/carbon composites made with different kinds of carbon fibers. J. Cent. South Univ. **19**, 1780 (2012)
20. H. Zhao, F. Yu, T.D. Bennett, H.N.G. Wadley, Morphology and thermal conductivity of yttria-stabilized zirconia coatings. Acta Mater. **54**(19), 5195 (2006)
21. J.G. Odhiambo, W. Li, Y. Zhao, C. Li, Porosity and its significance in plasma-sprayed coatings. Coatings **9**(7), 460 (2019)

22. S.T. Aruna, B. Arul Paligan, N. Balaji, V. Praveen Kumar, Properties of plasma sprayed yttria stabilized zirconia thermal barrier coating prepared from co-precipitation synthesized powder. Ceram. Int. **40**(7), 11157 (2014)
23. S.A. Sadeghi-Fadaki, K. Zangeneh-Madar, Z. Valefi, The adhesion strength and indentation toughness of plasma-sprayed yttria stabilized zirconia coatings. Surf. Coat. Technol. **204**(14), 2136 (2010)
24. R. Ghasemi, H. Vakilifard, Plasma-sprayed nanostructured YSZ thermal barrier coatings: thermal insulation capability and adhesion strength. Ceram. Int. **43**(12), 8556 (2017)
25. A.M. Khoddami, A. Sabour, S.M.M. Hadavi, Microstructure formation in thermally-sprayed duplex and functionally graded NiCrAlY/Yttria-Stabilized Zirconia coatings. Surf. Coat. Technol. **201**(12), 6019 (2007)
26. A. Nusair Khan, J. Lu, H. Liao, Effect of residual stresses on air plasma sprayed thermal barrier coatings. Surf. Coat. Technol. **168**(2), 291 (2003)
27. A.C. Karaoglanli, H. Dikici, Y. Kucuk, Effects of heat treatment on adhesion strength of thermal barrier coating systems. Eng. Fail. Anal. **32**, 16 (2013)
28. Abhinav, H.K. Kustagi, A.R. Shankar, Adhesion strength of plasma sprayed coatings—a review, in *Intelligent Manufacturing and Energy Sustainability*. ed. by A.N.R. Reddy, D. Marla, M. Simic, M.N. Favorskaya, S.C. Satapathy (Springer, Singapore, 2020), p.77
29. : Mechanisms of oxidation, in Introduction to the High Temperature Oxidation of Metals, edited by F. S. Pettit, G. H. Meier and N. Birks (Cambridge University Press, Cambridge, 2006), p. 39.
30. P.A. Selim, O. Dervis, O. Mecit, O. Yasin, D.K. Mert, G. Turgut, K.A. Cahit, Formation and growth behavior of TGO layer in TBCs with HVOF sprayed NiCr bond coat. Emerg. Mater. Res. **9**, 451 (2020)
31. J. Song, H. Qi, D. Shi, X. Yang, S. Li, Effect of non-uniform growth of TGO layer on cracking behaviors in thermal barrier coatings: a numerical study. Surf. Coat. Technol. **370**, 113 (2019)